

Dielectric functions and collective excitations in MgB_2

V. P. Zhukov¹, V. M. Silkin¹, E. V. Chulkov^{1,2}, and P. M. Echenique^{1,2}

¹*Donostia International Physics Center (DIPC), 20018 San Sebastián/Donostia, Basque Country, Spain*

²*Departamento de Física de Materiales and Centro Mixto CSIC-UPV/EHU, Facultad de Ciencias Químicas, Universidad del País Vasco/Euskal Herriko Unibertsitatea, Apdo. 1072, 20018 San Sebastián/Donostia, Basque Country, Spain*

(November 1, 2018)

The frequency- and momentum-dependent dielectric function $\epsilon(\mathbf{q}, \omega)$ as well as the energy loss function $\text{Im}[-\epsilon^{-1}(\mathbf{q}, \omega)]$ are calculated for intermetallic superconductor MgB_2 by using two *ab initio* methods: the plane-wave pseudopotential method and the tight-binding version of the LMTO method. We find two plasmon modes dispersing at energies ~ 2 -8 eV and ~ 18 -22 eV. The high energy plasmon results from a free electron like plasmon mode while the low energy collective excitation has its origin in a peculiar character of the band structure. Both plasmon modes demonstrate clearly anisotropic behaviour of both the peak position and the peak width. In particular, the low energy collective excitation has practically zero width in the direction perpendicular to boron layers and broadens in other directions.

74.70.Ad, 71.45.Gm, 74.24.Jb

After the discovery of superconductivity in the MgB_2 compound with the transition temperature $T_c \sim 39K$ [1] much effort has been devoted to understanding the mechanism of the superconductivity [2–11] as well as to studying different electronic and atomic characteristics of this compound. Among these characteristics are the superconducting gap [3,12,13], the crystal structure and its influence on T_c [1,2,14–16], band structure [4,5,17–19] and the Fermi surface [4], lattice vibrations [6,9,20,21] as well as thermodynamic and transport properties [22]. Recently Voelker *et al* [8] explored collective excitations very near the Fermi level by using a simple band structure model and found the plasmon acoustic mode at very small momenta ($q \simeq 0.01 \text{ a.u.}^{-1}$) and low energies ($\omega \simeq 0.01 \text{ eV}$). Here we study collective excitations in MgB_2 for different momenta and energies, namely, for $q \geq 0.1 \text{ a.u.}^{-1}$ and $\omega \geq 2 \text{ eV}$. We report first-principle calculations for the real, $\epsilon_1(\mathbf{q}, \omega)$, and imaginary, $\epsilon_2(\mathbf{q}, \omega)$, part of the dielectric function as well as the energy loss function $\text{Im}[-\epsilon^{-1}(\mathbf{q}, \omega)]$. As a result of the calculation two plasmon modes and a few features arising from interband transitions are obtained.

MgB_2 crystallizes in the so-called AlB_2 structure in which B atoms form graphitelike honeycomb layers that alternate with hexagonal layers of Mg atoms. The magnesium atoms are located at the center of hexagons formed by borons and donate their electrons to the boron planes. Similar to graphite MgB_2 exhibits a strong anisotropy in the B - B lengths: the distance between the boron planes is significantly longer than in-plane B - B distance. We use this resemblance between graphite and MgB_2 in order to clear up the origin of plasmon peaks in MgB_2 by comparing the calculated energy loss function features with those obtained from EELS measurements for graphite and single-wall carbon nanotubes (SWCN) [26,27]. To shed more light on the problem we also evaluate the dielectric functions and the energy loss spectra for the MgB_2 crystal structure with the Mg atoms re-

moved (this hypothetical crystal structure is designated as B_2).

Information on the energy lost by electrons in their interactions with metals is carried by the dynamical structure factor $S(\mathbf{q}, \omega)$ which is related by the fluctuation-dissipation theorem to the energy loss function $\text{Im}[-\epsilon_{00}^{-1}(\mathbf{q}, \omega)]$. To calculate the inverse dielectric function we invoke the random phase approximation (RPA) where $\epsilon^{-1}(\mathbf{q}, \omega)$ is defined as (in symbolic form) $\epsilon^{-1} = 1 + v_c(1 - \chi^0 v_c)^{-1} \chi^0$, where v_c is the bare Coulomb potential and χ^0 is the density response function of the non-interacting electron system. The dielectric function is related to χ^0 as $\epsilon = 1 - v_c \chi^0$. The energy loss function may be obtained by inverting the first matrix element of ϵ that leads to neglecting short-range exchange and correlation effects or directly from ϵ^{-1} when these effects are included. We have computed the energy loss function by using both of these approaches and found that the inclusion of the local field effects leads to negligible changes of both the width and energy of the plasmon peaks. In the calculation of the density response matrix $\chi_{\mathbf{GG}'}^0(\mathbf{q}, \omega)$ we have used two different first-principle methods: the plane wave pseudopotential method [23] and the tight-binding version of the LMTO method [24,25].

In Figs. 1a and 1b we show the evaluated band structure of MgB_2 and B_2 along the symmetry directions. In general, these band structures are quite similar. The distinctions between them in the vicinity of the Fermi level (E_F) are due to the lower position of E_F relative to the σ band in the ΓA direction for B_2 . The states of this band, which are of $p_{x,y}$ symmetry, are degenerate in ΓA and their charge density is located in B layer showing a clear 2D character. This character leads to weaker interactions between the B layers and to smaller dispersion of the σ band along ΓA in B_2 . The p_z band which is occupied at Γ in MgB_2 becomes unoccupied at Γ in B_2 . In Figs. 2a and 2b we present the momentum dependence of the energy loss function in the ΓA , ΓK and

ΓM directions. In MgB_2 we have found two plasmon modes. The higher collective excitation mode originates from the free electron like excitation mode with energy $\omega_{p1}=19.1$ eV that corresponds to the electron density parameter $r_s=1.82$ a.u. of MgB_2 . This free electron like mode is transformed into two separated submodes ω_{p1}^{xy} and ω_{p1}^z in a real crystal. One of them is very isotropic in the hexagonal plane (the ΓK and ΓM directions) and disperses linearly up for momenta $q \geq 0.2$ a.u., while another one, in the ΓA direction, has smaller energy and is nearly constant. Because of limitations of the calculation methods and a large width of the energy loss peaks at small momenta we could not determine accurately the plasmon peak position in this region. Therefore we define the plasmon energy at the $\bar{\Gamma}$ point by extrapolation of the computed plasmon dispersions at $q \geq 0.2$ a.u. This extrapolation results in $\omega_{p1}^{xy}=19.4$ eV and $\omega_{p1}^z=18.8$ eV in good agreement with the free electron gas value ω_{p1} . The width, Δ_{p1} , of both these energy loss peaks decreases with the increasing momentum, and the Δ_{p1}^z width decreases faster than Δ_{p1}^{xy} .

A different behavior is shown by the low-energy loss function peak which disperses linearly up in both the ΓA direction and in the hexagonal plane. In the ΓA direction, at $q_{\perp} \sim 0.1$ a.u.⁻¹, the peak is very narrow, $\Delta_{p2}^z \sim 0.01$ eV, that can be seen in the very small value of ϵ_2 in the energy interval around the peak position where $\epsilon_1=0$ (Figs. 3a and 3b). In particular, for $q_{\perp}=0.12$ a.u.⁻¹ this interval is between 1 and 5 eV (Fig. 3a) and the energy loss peak is located at 2.9 eV. On changing the momentum to the A point this interval becomes more narrow and moves to higher energies (Fig. 3c). At small momenta the first peak of $\text{Im}[-\epsilon_{00}(\mathbf{q}, \omega)]$ placed in the energy interval 0-1 eV is determined by intraband transitions within the two σ bands in the x, y plane around the ΓA direction, while the second peak located at 5.4 eV (Fig. 3a) is determined by the interband $\sigma - \pi$ transitions in the KM , AH , and AL directions. So, the low energy plasmon excitation corresponds to electron excitations in the σ bands and one can define it as the σ plasmon. In the hexagonal plane, in the ΓK direction, the low energy EELS peak broadens (Fig. 4a) and disperses linearly up on going from the Γ point to K. In the ΓM direction the plasmon peak disperses similar to that in the ΓK one showing a nearly ideal isotropy in the hexagonal plane. However, it becomes smaller and wider on going from Γ to M and vanishes finally at $q \simeq 0.8 |\Gamma M|$. Comparing the plasmon energies obtained from the LMTO and pseudopotential calculations one can find only a small difference of ~ 0.1 eV between them. For instance, at $q=0.2$ a.u.⁻¹ the LMTO ω_{p2}^z is slightly smaller than the pseudopotential one and *vice versa* for larger momenta. This slight difference results in different energy loss peak positions at Γ : the extrapolation of both plasmon energies ω_{p2}^{xy} and ω_{p2}^z calculated for $q \geq 0.1$ a.u.⁻¹ to the Γ point

gives $\omega_{p2}^z=1.8$ eV, $\omega_{p2}^{xy}=2.0$ eV (LMTO) and $\omega_{p2}^z=2.2$ eV, $\omega_{p2}^{xy}=2.4$ (pseudopotential). We estimate the accuracy of these values to be better than 0.2 eV.

Besides two plasmon modes we have obtained four small features in $\text{Im}[-\epsilon_{00}^{-1}(\mathbf{q}, \omega)]$ that correspond to interband excitations. It is difficult to find out what transitions are responsible for these features, nevertheless we show them in Fig. 2a. One of them arises at $q \simeq 0.1$ a.u.⁻¹ at an energy of ≈ 2 eV in the hexagonal plane, another one occurs at $q \geq 0.4$ a.u.⁻¹ in the ΓM direction at an energy of $\simeq 4$ eV and the other two small features arise in the ΓA direction for $q=0.1-0.25$ a.u.⁻¹ at energies of 10 eV and 13 eV, respectively.

In Fig. 2b we show the momentum dependence of the energy loss function calculated for the hypothetical crystal structure B_2 . In general, the energy loss function in B_2 shows relatively similar features to those in MgB_2 , though there are some important distinctions. In particular, all collective excitations including two plasmon modes manifest a smaller dispersion in the ΓA direction. This effect is a direct consequence of a weaker interactions between adjacent layers of boron in B_2 compared to MgB_2 . Another distinction is that all features in the energy loss function in B_2 are much clearer than those in MgB_2 (Figs. 3a-3c and 4a-4c). One exception is the high energy plasmon mode. The third distinction is that B_2 has more features in $\text{Im}[-\epsilon_{00}^{-1}(\mathbf{q}, \omega)]$ than does MgB_2 . The low energy plasmon mode extrapolation to the Γ point gives $\omega_{p2}^z=4.1$ eV which is ~ 2 eV higher than that in MgB_2 . This shift in energy is due to the higher energy position of the second maximum of $\text{Im}[\epsilon_{00}]$ (Fig. 3a). While the position of the first peak of $\text{Im}\epsilon$ in B_2 nearly coincides with that in MgB_2 the second peak is moved by 2 eV to higher energies. Via the Hilbert transform (Kramers-Kronig relation) it also moves the node of ϵ_1 to higher energy. Despite some quantitative distinctions between the energy loss functions in MgB_2 and B_2 one can conclude that mostly the features of the excitation spectrum of MgB_2 can be derived, with the relevant corrections, from those of the hypothetical crystal B_2 .

The two plasmon modes similar to those obtained in MgB_2 were also observed in EELS experiments for graphite and SWCN [26,27] which are even more anisotropic than MgB_2 . The upper plasmon mode which has larger energy in graphite and SWCN than in MgB_2 (near the Γ point $\omega_{p1}^{xy} \simeq 21$ eV (SWCN) and $\omega_{p1}^{xy} \simeq 26$ eV (graphite)) [27] also results from excitations of all valence electrons. The lower plasmon mode ω_{p2}^{xy} shows a linear dependence on momentum, like that in MgB_2 , with energies $\omega_{p2}^{xy} \simeq 5$ eV (SWCN) and $\omega_{p2}^{xy} \simeq 6.5$ eV (graphite) [27] at Γ . But in contrast to SWCN and graphite where ω_{p2}^{xy} represents the collective excitation of the π -electron system [26–28] in MgB_2 this mode is a result of the collective excitation of the σ -electron system. The different origin of the low-energy plasmon mode in MgB_2/B_2 and graphite/SWCN can be qualitatively understood from

the Fermi energy (E_F) position. In graphite the Fermi level is pinned by π -electrons in the KH direction. In MgB_2 and B_2 with a smaller number of electrons per atom the Fermi level is pinned by σ -electrons. So, low-energy excitations in MgB_2 and in B_2 are expected to be derived from the σ -band electrons.

In conclusion, we have performed the first-principle calculations of the dielectric functions $\epsilon_1(\mathbf{q}, \omega)$ and $\epsilon_2(\mathbf{q}, \omega)$ as well as the energy loss function $\text{Im}[-\epsilon^{-1}(\mathbf{q}, \omega)]$. The calculations reveal the two plasmon modes in MgB_2 and B_2 and a few interband collective excitations. The low energy plasmon mode corresponding to the excitations of electrons in the σ bands shows a very anisotropic behavior of the peak width. The energy loss spectrum of MgB_2 can be derived, with the relevant corrections, from that of the hypothetical crystal structure B_2 .

We thank R.H.Ritchie and A.Bergara for helpful discussions. This work was partially supported by the Basque Country University, Basque Hezkuntza Saila, and Iberdrola S.A.

After the submission of this paper first-principles calculations of collective excitations in MgB_2 have also been presented by Wei Ku *et al.* [29].

[1] J. Nagamatsu *et al.*, Nature **410**, 63 (2001).
[2] S. L. Bud'ko *et al.*, Phys. Rev. Lett. **86**, 1877 (2001).
[3] T. Takahashi *et al.*, cond-mat/0103079.
[4] J. Kortus *et al.*, Phys. Rev. Lett. **86**, 4656 (2001).
[5] J. M. An and W. E. Pickett, Phys. Rev. Lett. **86**, 4366 (2001).
[6] Y. Kong *et al.*, cond-mat/0102499.
[7] J. E. Hirsch and F. Marsiglio, cond-mat/0102479.
[8] K. Voelker, V. I. Anisimov, and T. M. Rice, cond-mat/0103082.
[9] R. Osborn *et al.*, cond-mat/0103064.
[10] E. Bascones and F. Guinea, cond-mat/0103190.
[11] A. Y. Liu, I. I. Mazin, and J. Kortus, cond-mat/0103570.
[12] G. Karapetrov *et al.*, Phys. Rev. Lett. **86**, 4374 (2001).
[13] B. Gorshunov *et al.*, cond-mat/0103164.
[14] J. S. Slusky *et al.*, Nature, **410**, 343 (2001).
[15] J. D. Jorgensen, D. G. Hinks, and S. Short, cond-mat/0103069.
[16] E. Saito *et al.*, J. Phys.: Condens. Matter, **13**, L267 (2001).
[17] K. D. Belashchenko, M. van Schilfgaarde, and V. P. Antropov, con-mat/0102290.
[18] G. Satta *et al.*, cond-mat/0102358.
[19] N. I. Medvedeva *et al.*, cond-mat/0103157.
[20] T. J. Sato, K. Shibata, and Y. Takano, cond-mat/0102468.
[21] K.-P. Bohnen, R. Heid, and B. Renker, cond-mat/0103319.
[22] D. K. Finnemore *et al.*, Phys. Rev. Lett. **86**, 2420 (2001).

[23] The Mg and B pseudopotentials were generated according to N. Troullier and J. L. Martins, Phys. Rev. B **43**, 1993 (1991). Convergent results for one-electron energies and wave functions were obtained with a 25 Ry plane-wave cut-off. In the evaluation of the density response function we used ~ 80 bands (up to 100 eV) above E_F and three grids which include $\sim 13,000$, $\sim 27,000$, $\sim 47,000$ \mathbf{k} points. The convergence was already achieved at $\sim 13,000$ points.
[24] O. K. Andersen, Z. Pawłowska, and O. Jepsen, Phys. Rev. B **34**, 5253 (1984).
[25] F. Aryasetiawan and O. Gunnarson, Rept. Progr. Phys. **61**, 237 (1998).
[26] R. Kuzuo *et al.*, Jpn. J. Appl. Phys. **33**, L1316 (1994).
[27] T. Pichler *et al.*, Phys. Rev. Lett. **80**, 4729 (1998).
[28] R. Ahuja *et al.*, Phys. Rev. B **55**, 4999 (1997).
[29] Wei Ku, W. E. Pickett, R. T. Scalettar, and A. G. Eguiluz, cond-mat/0105389.

FIG. 1. Calculated energy band structure of a) MgB_2 and b) B_2 along the symmetry directions. σ and π denote the boron bands of $p_{x,y}$ and p_z character, respectively.

FIG. 2. (color) Dispersion of the plasmon modes (filled circles) and of the features (triangles) for a) MgB_2 and b) B_2 along the symmetry directions: ΓA (green), ΓK (red), and ΓM (blue).

FIG. 3. (color) Real (dashed lines) and imaginary (solid lines) parts of the dielectric function $\epsilon_{\mathbf{G}\mathbf{G}}(\mathbf{q}, \omega)$ along the ΓA direction for $\mathbf{G}=0$ and $\mathbf{q}=(0,0,\alpha)(2\pi/c)$: a) $\alpha=1/8$, b) $\alpha=1/4$, c) $\alpha=1/2$ (A point). The energy loss function is shown in the insert. The red (blue) lines represent MgB_2 (B_2).

FIG. 4. (color) Real (dashed lines) and imaginary (solid lines) parts of the dielectric function $\epsilon_{\mathbf{G}\mathbf{G}}(\mathbf{q}, \omega)$ along the ΓK direction for $\mathbf{G}=0$ and $\mathbf{q}=(\alpha,0,0)(2\pi/a)$: a) $\alpha=1/9$, b) $\alpha=1/3$, c) $\alpha=2/3$ (K point). The energy loss function is shown in the insert. The red (blue) lines represent MgB_2 (B_2).

Fig. 1a

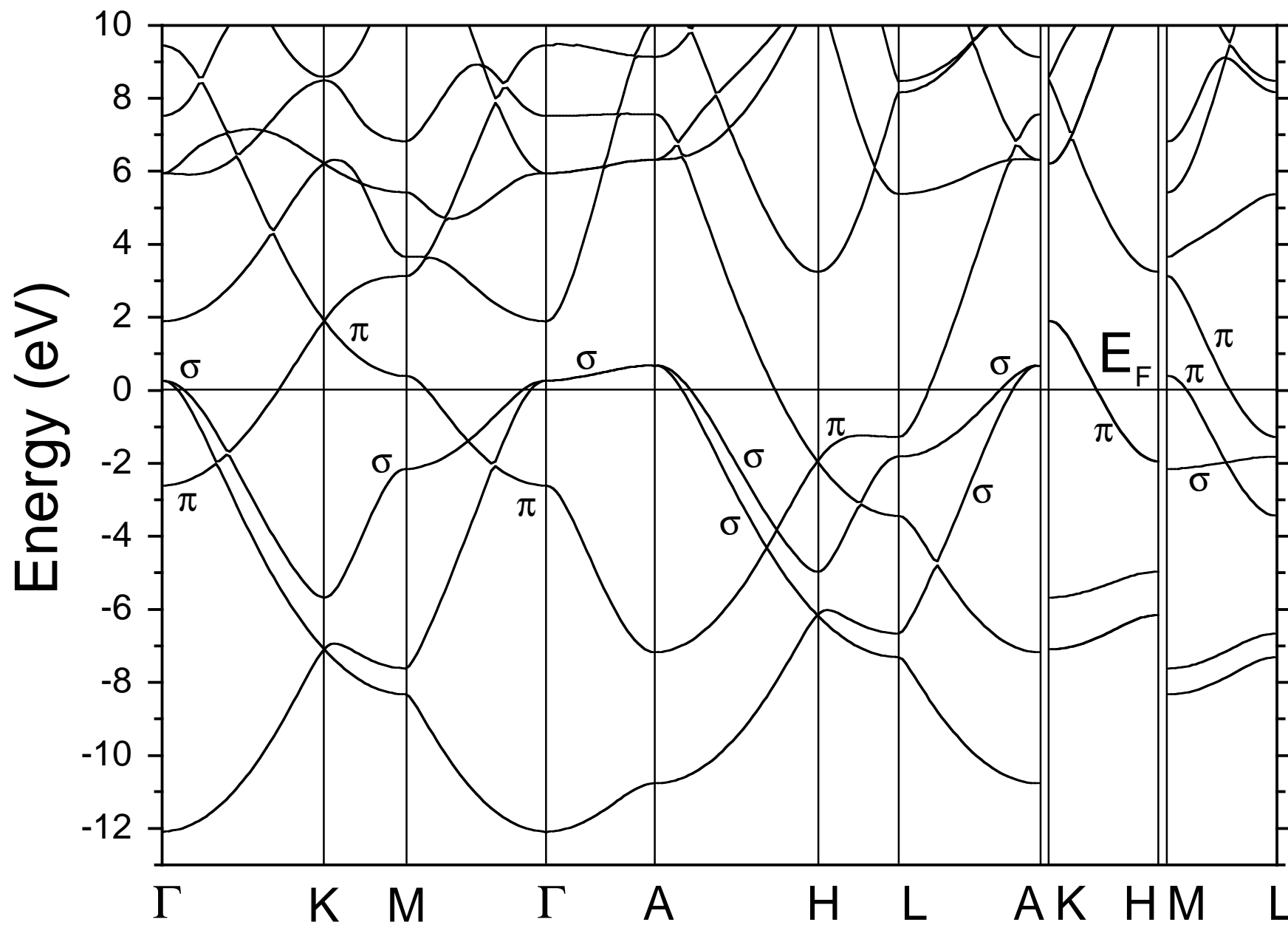


Fig. 1b

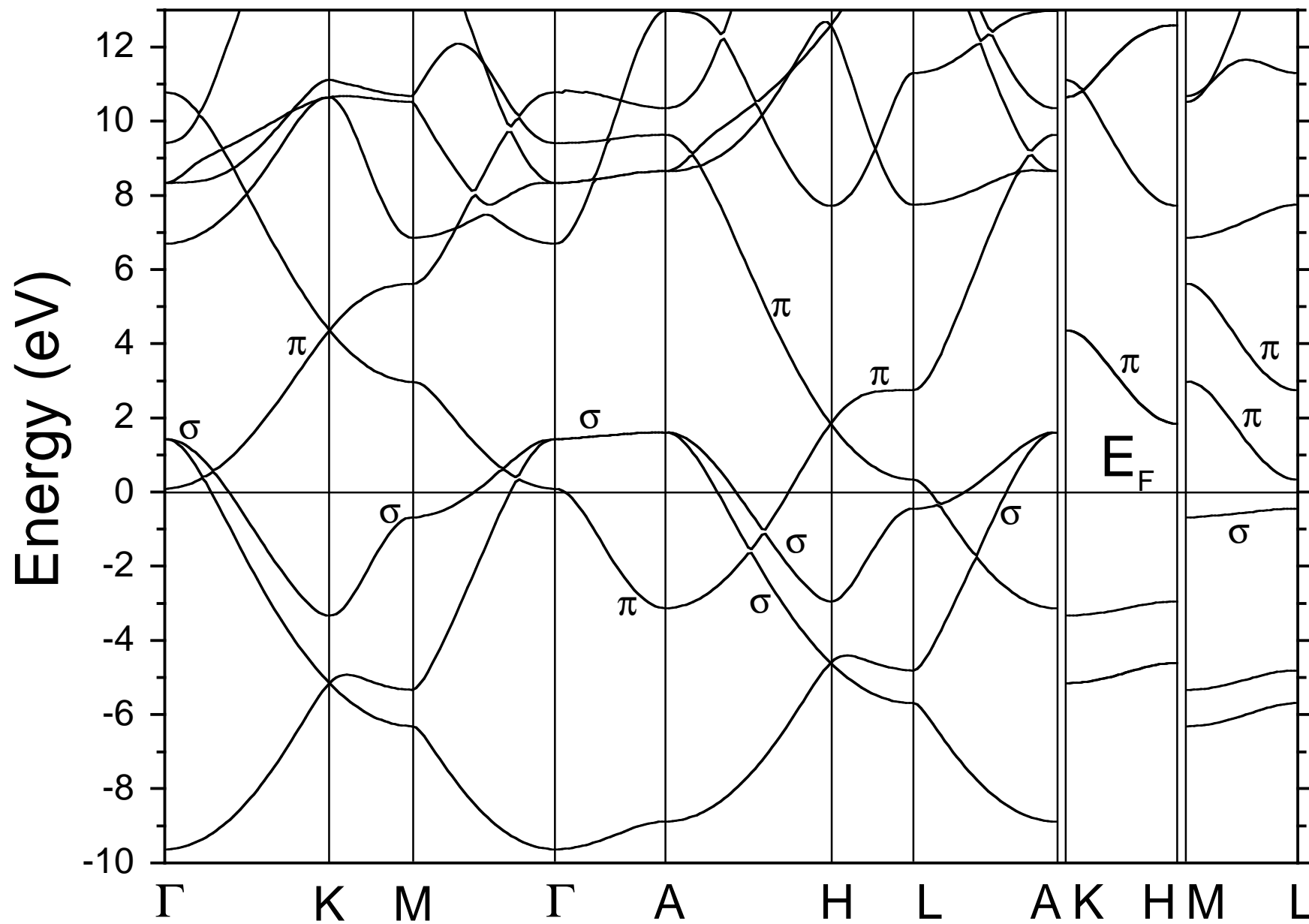


Fig. 2a

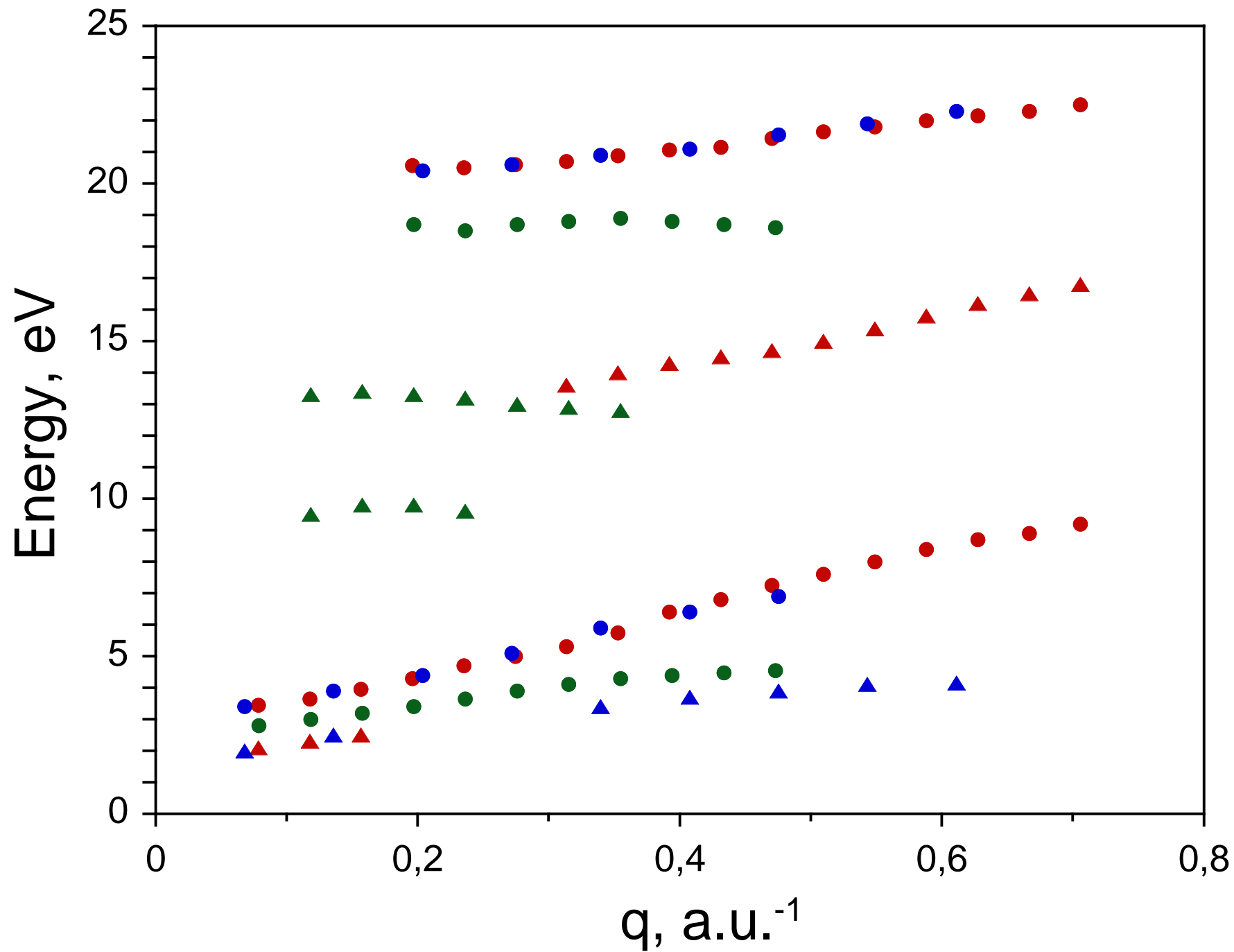


Fig. 2b

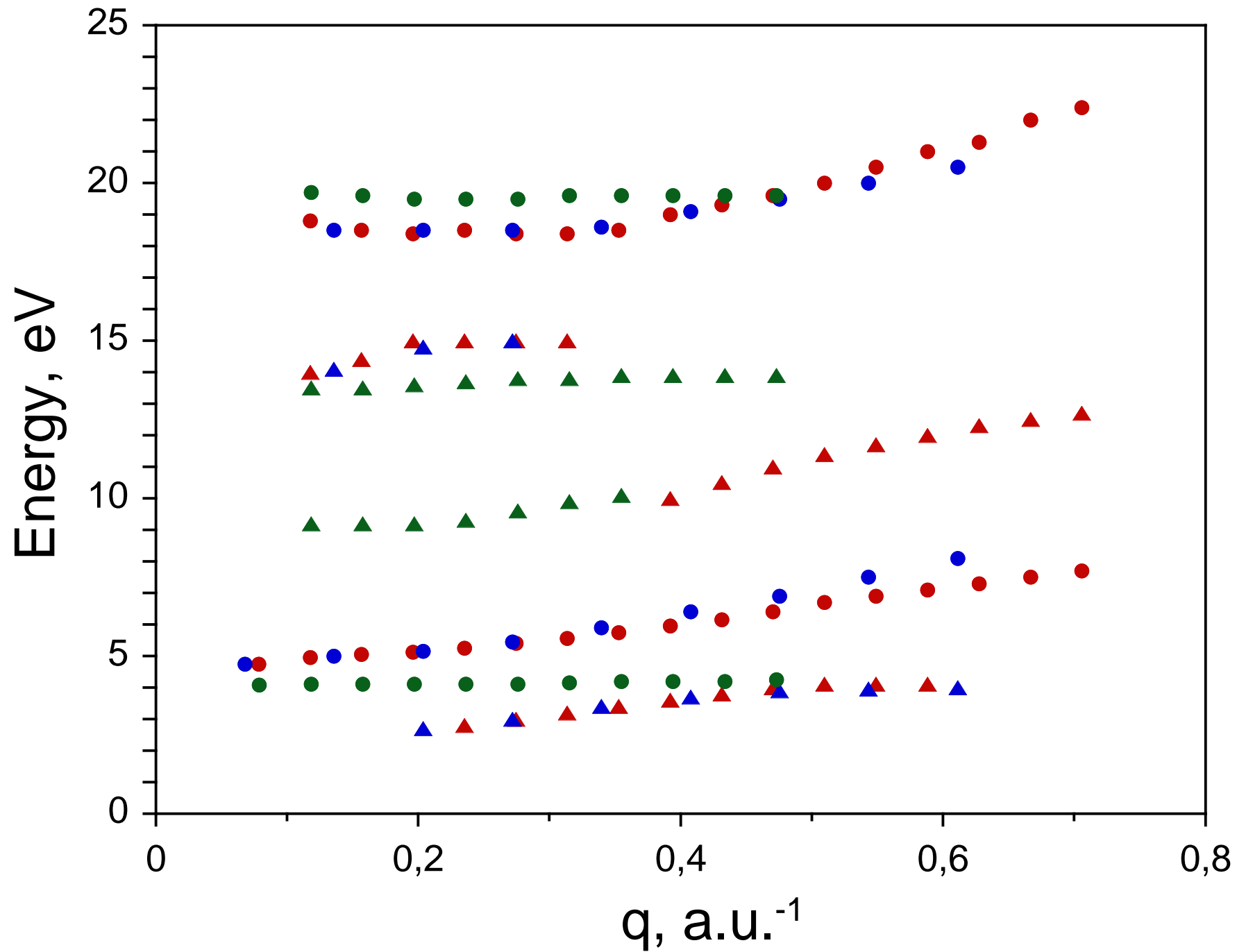


Fig. 3a

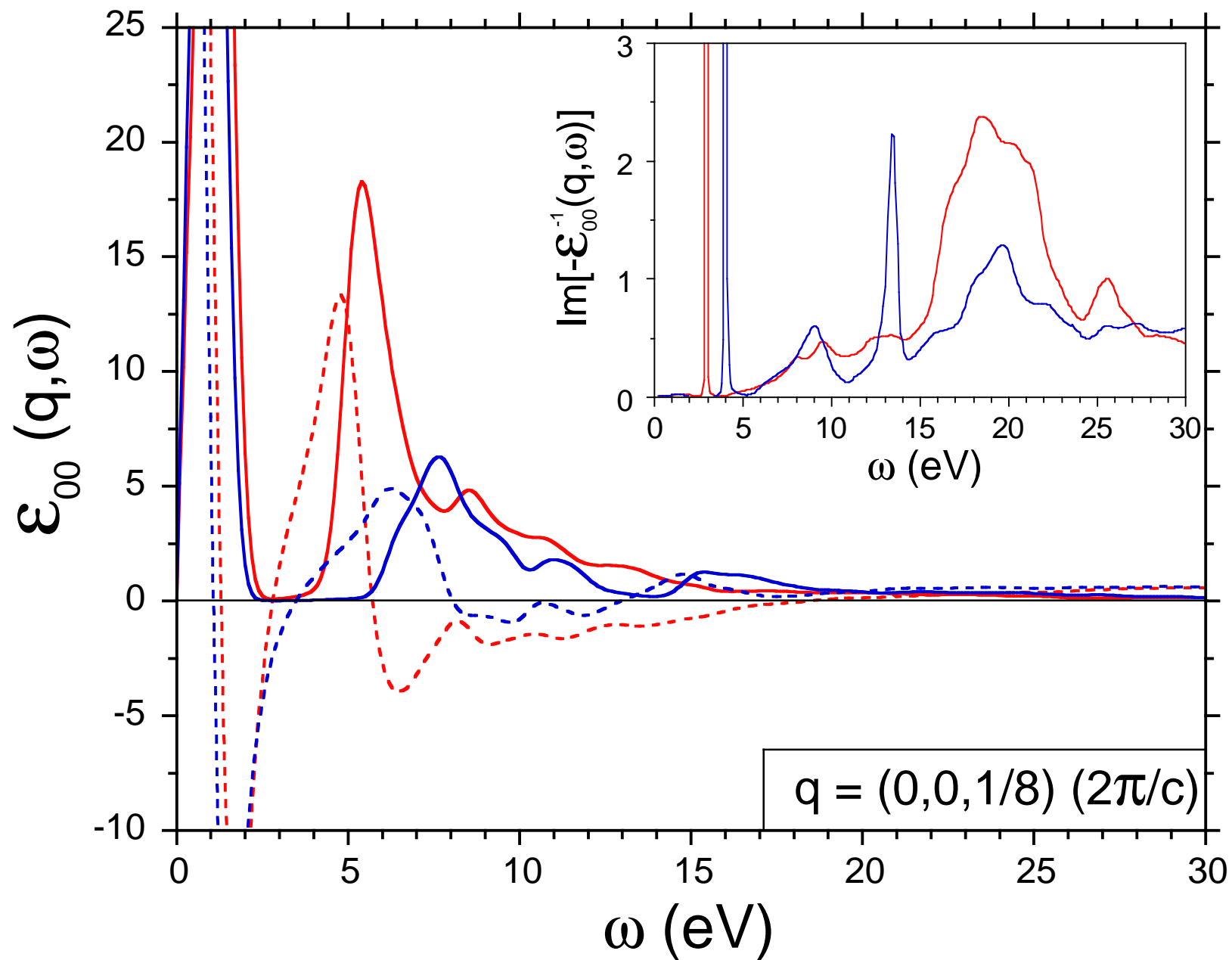


Fig. 3b

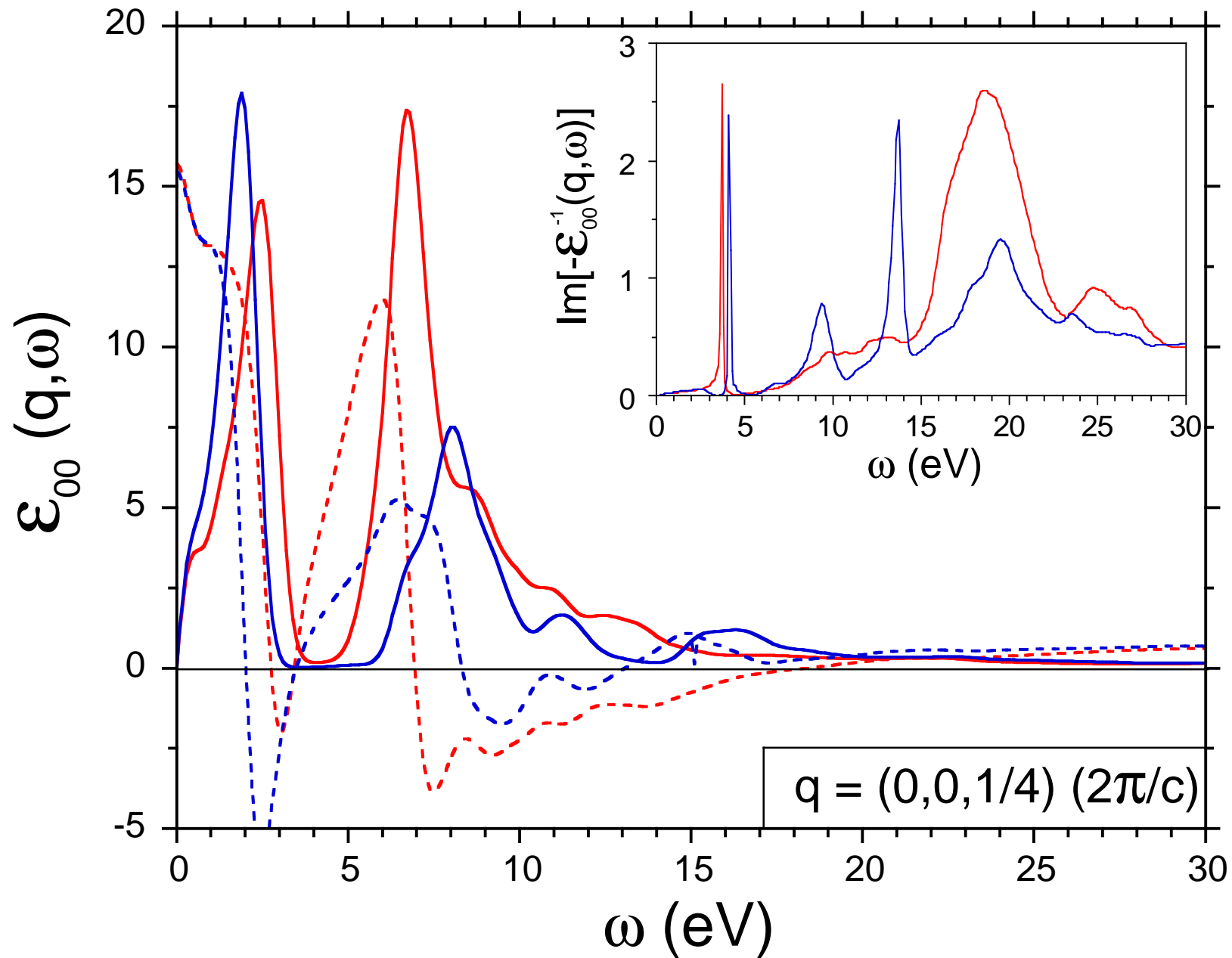


Fig. 3c

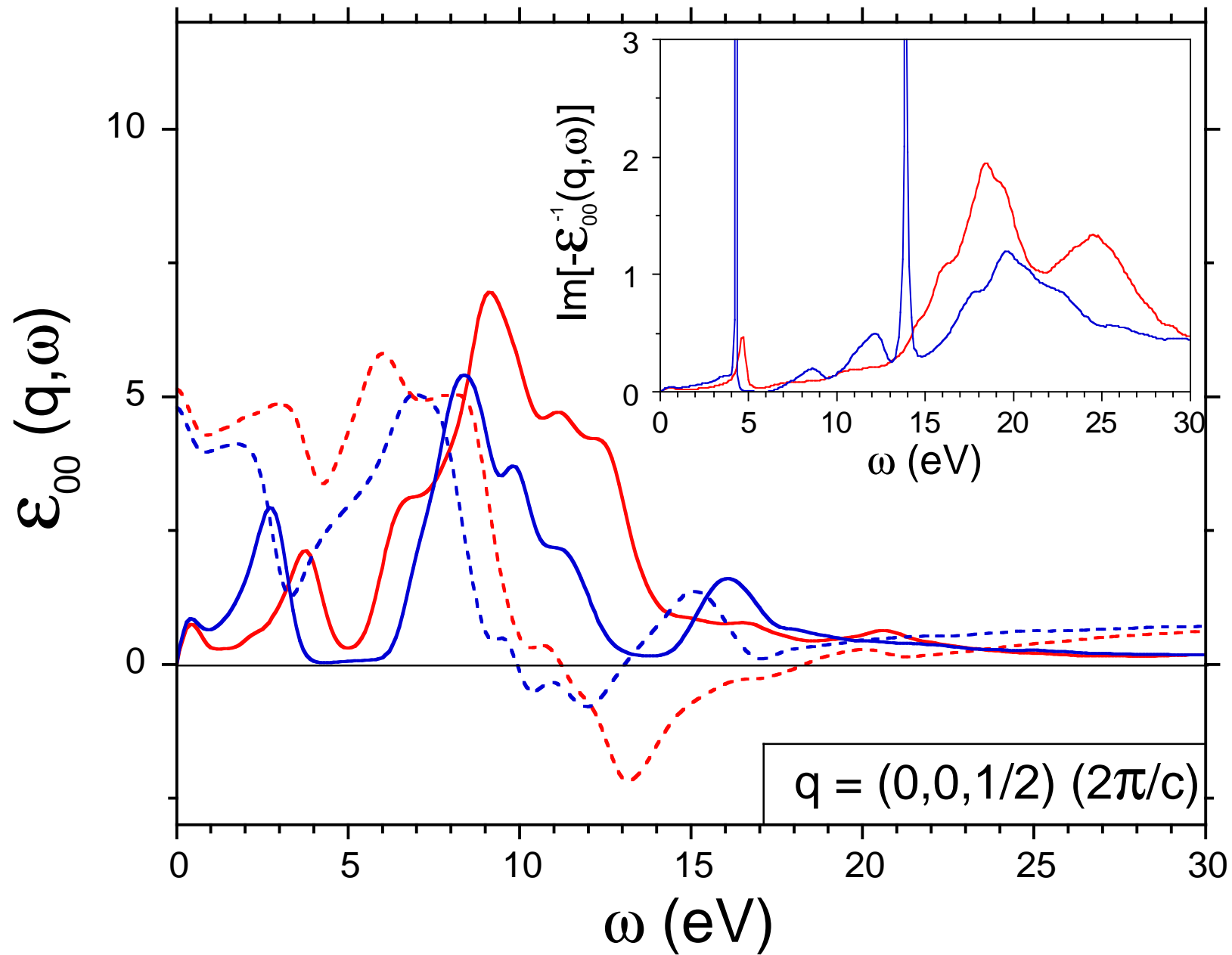


Fig. 4a

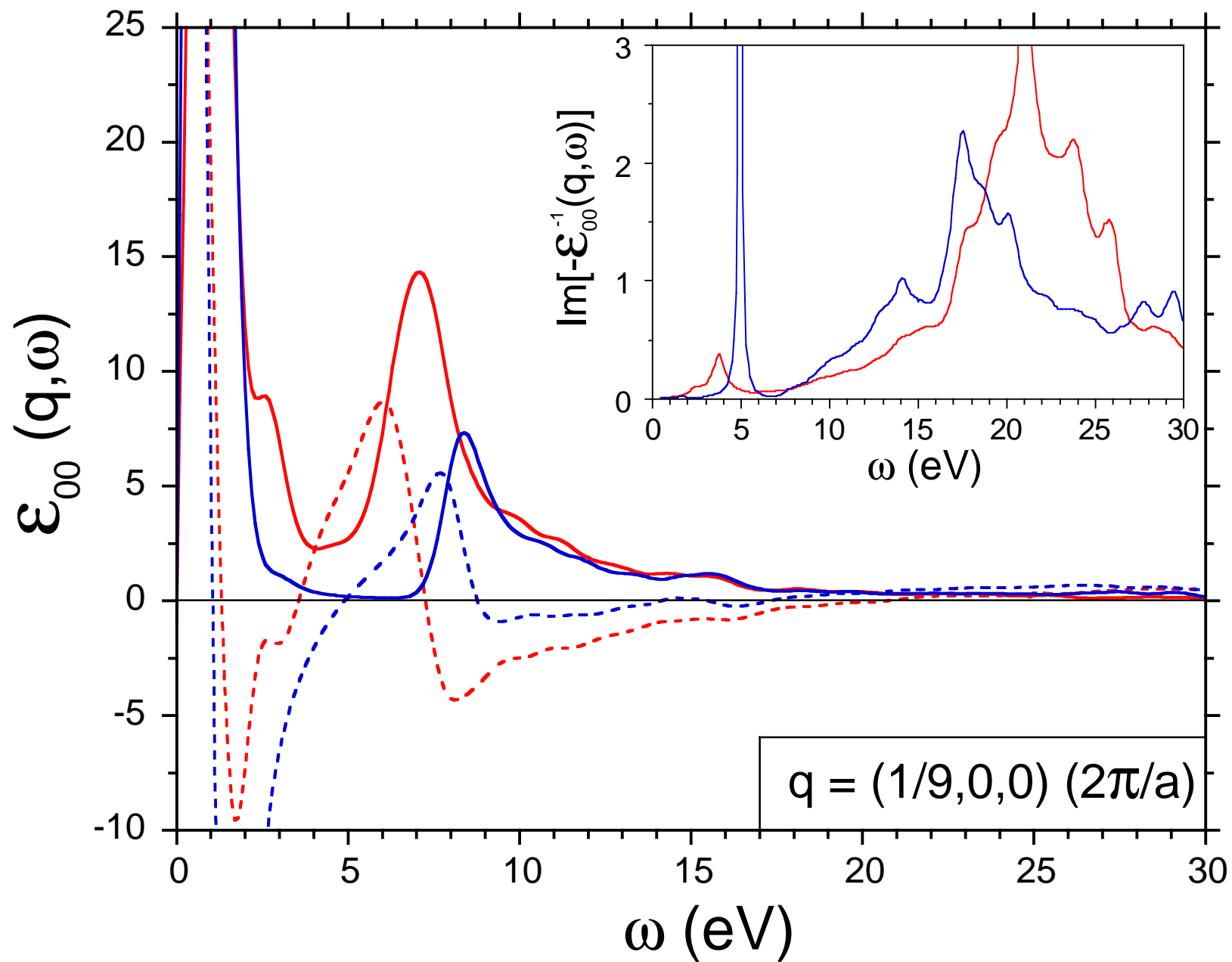


Fig. 4b

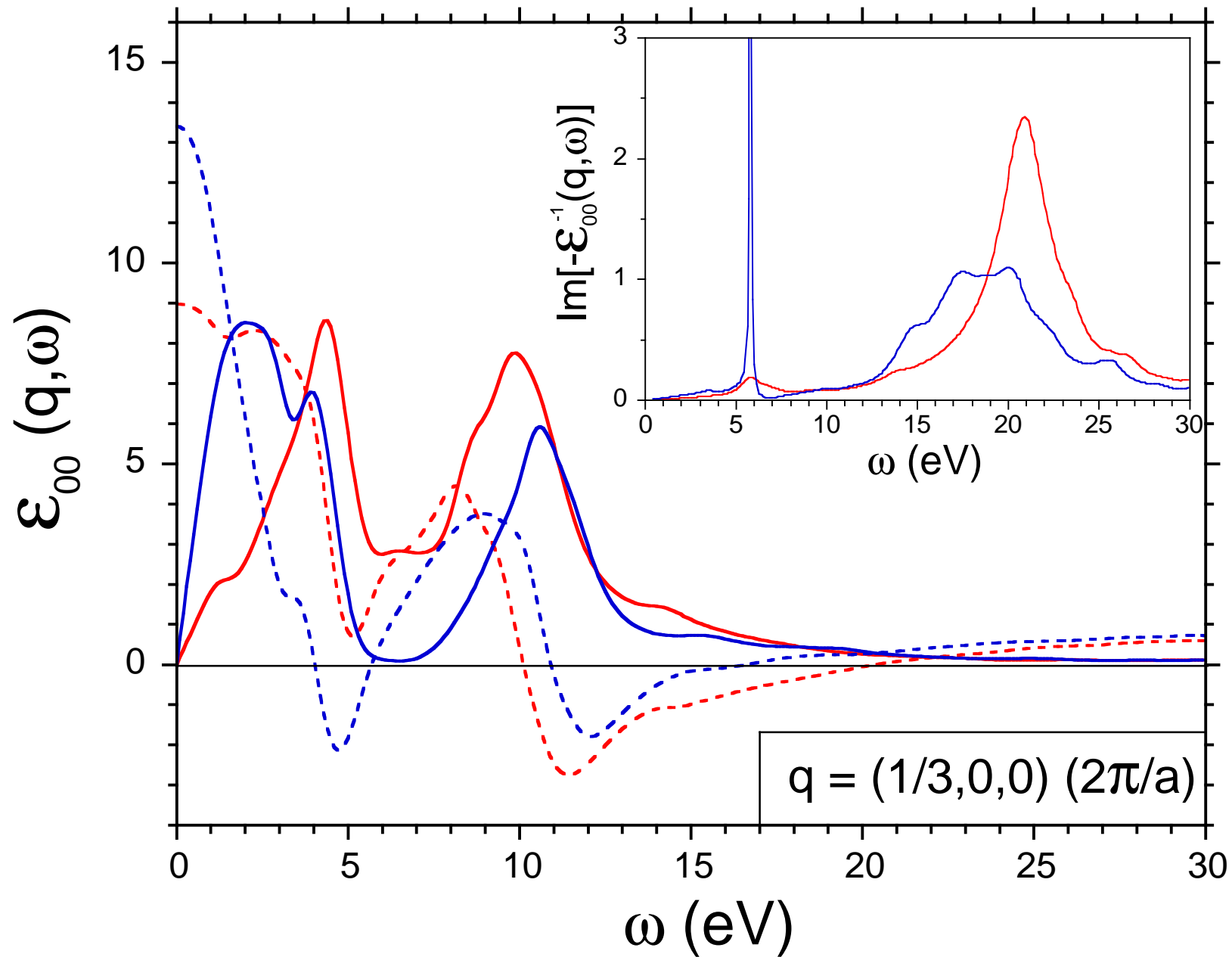


Fig. 4c

